

StableMoFusion: Towards Robust and Efficient Diffusion-based Motion Generation Framework

Yiheng Huang¹, Hui Yang², Chuanchen Luo³, Yuxi Wang³, Shibiao Xu¹, Zhaoxiang Zhang³, Man Zhang^{*1}, and Junran Peng^{*3}

¹Beijing University of Posts and Telecommunications

²CAIR, HKISI, CAS

³Institute of Automation, Chinese Academy of Science

Abstract

Thanks to the powerful generative capacity of diffusion models, recent years have witnessed rapid progress in human motion generation. Existing diffusion-based methods employ disparate network architectures and training strategies. The effect of the design of each component is still unclear. In addition, the iterative denoising process consumes considerable computational overhead, which is prohibitive for real-time scenarios such as virtual characters and humanoid robots. For this reason, we first conduct a comprehensive investigation into network architectures, training strategies, and inference processes. Based on the profound analysis, we tailor each component for efficient high-quality human motion generation. Despite the promising performance, the tailored model still suffers from foot skating which is an ubiquitous issue in diffusion-based solutions. To eliminate footskate, we identify foot-ground contact and correct foot motions along the denoising process. By organically combining these well-designed components together, we present StableMoFusion, a robust and efficient framework for human motion generation. Extensive experimental results show that our StableMoFusion performs favorably against current state-of-the-art methods. Project page: <https://h-y1heng.github.io/StableMoFusion-page/>.

1. Introduction

Human motion generation aims to generate natural, realistic, and diverse human motions, which could be used for animating virtual characters or manipulating humanoid robots to imitate vivid and rich human movements without long-time manual motion modeling and professional

*Corresponding authors: ManZhang (zhangman@bupt.edu.cn) and Junran Peng (jrpeng4ever@126.com)

Table 1. StableMoFusion achieves superior performance on motion generation compared to other state-of-the-art methods. Lower FID and higher R Precision mean, the better.

Method	FID↓	R Precision (top3)↑
MDM [28]	0.544	0.611
MLD [3]	0.473	0.772
MotionDiffuse [37]	0.630	0.782
ReMoDiffuse [38]	0.103	0.795
StableMoFusion (Ours)	0.098	0.841

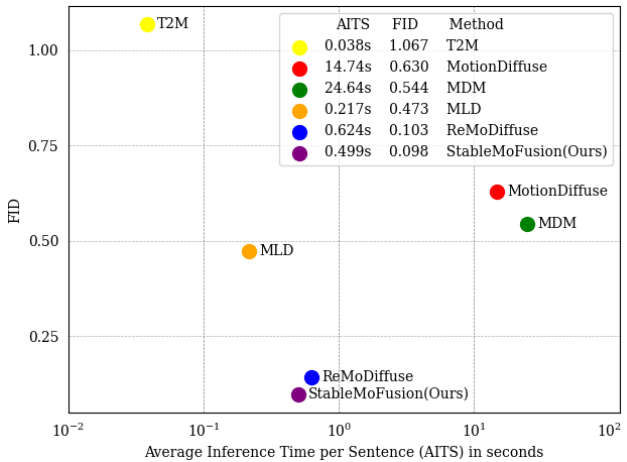


Figure 1. Comparison of the inference time costs on motion generation. The closer the model is to the origin, the better.

skills[1, 4, 37]. It shows great potential in the fields of animation, video games, film production, human-robot interaction and *etc.* Recently, the application of diffusion models to human motion generation has led to significant improvements in the quality of generated motions [3, 28, 37].

Despite the notable progress made by diffusion-based motion generation methods, its development is still hindered by several fragmented and underexplored issues: 1) **Lack of Systematic Analysis**: these diffusion-based motion generation work usually employ different network architectures and training pipelines, which hinders cross-method integration and the adoption of advancements from related domains. 2) **Long Inference Time**: due to the time-consuming iterative sampling process, most existing methods are impractical for applications with virtual characters and humanoid robots, where real-time responsiveness is crucial. 3) **Footskate Issue**: foot skating (footskate) in generated motions remains a major concern. This significantly undermines the quality of generated motions and limits their practical applicability.

Therefore, in order to fill these research gaps and enhance the effectiveness and reliability of diffusion-based motion generation in practical applications, our study conducts a comprehensive and systematic investigation into network architectures, training strategies, and inference process. Our investigation is specifically directed towards text conditional motion generation, as text prompts are arguably the most promising format for practical application and the most convenient input modality among various conditional signals. Ultimately, we present a robust and efficient framework for diffusion-based motion generation, called *StableMoFusion*, as illustrated in [Figure 2](#).

In *StableMoFusion*, we use Conv1D UNet with AdaGN and linear cross-attention as the motion-denoising network, and improve its generalization capability with GroupNorm tweak. During training, two effective strategies were employed to enhance the network’s ability to generate motion. During inference, we use four training-free acceleration tricks to achieve efficient inference. Furthermore, we present a footskate cleanup method based on a mechanical model and optimization.

Extensive experiments demonstrate that *StableMoFusion* achieves an excellent trade-off between text-motion consistency and motion quality compared to other state-of-the-art methods, as shown in [Table 1](#). Meanwhile, *Stablemofusion*’s efficient inference process notably reduces the minimum number of iterations required for generation from 1000 to 10, as well as shorter inference times than methods of about the same performance, achieving an average inference time of 0.5 seconds on the Humanm3D test set, as shown in [Figure 1](#). In addition, our footskate cleanup method within diffusion framework sizably solves the foot skating problem of motion generation as shown in [Section 5.4](#).

Our major contributions can be summarized as follows:

- We perform a systematic evaluation and analysis on the design of each component in the diffusion-based motion generation pipeline, including network architectures,

training strategies, and inference process.

- We propose an effective mechanism to eliminate foot skating which is a comment issue in current methods.
- By consolidating these well-designed components, we present a robust and efficient diffusion-based motion generation framework named *StableMoFusion*. Extensive experiments demonstrate its superiority in text-motion consistency and motion quality.

2. Related Work

2.1. Motion Diffusion Generation

In recent years, the application of diffusion models to human motion generation has led to significant improvements in the quality of generated motions. MotionDiffuse [37] softly fuses text features into diffusion-based motion generation through cross-attention. MDM [28] experimented with the separate Transformer encoder, decoder, GRU as denoising networks, respectively. PyhsDiff [35] incorporates physical constraints to generate more realistic motions; Prior MDM [24] uses diffusion priors to allow the model to be applied to specific generative tasks; MLD [3] utilizes the latent space of VAE to speed up diffusion generation; ReMoDiffuse [38] uses a retrieval mechanism to enhance the motion diffusion model. All of these methods use Transformer-based network structure, while MoFusion [4] and GMD [13] use Conv1D UNet for motion diffusion generation.

Our work towards a more robust and efficient diffusion-based motion generation framework through a comprehensive investigation into network architectures, training strategies, and inference process. It also addresses the practical application challenges of long inference time and footskate phenomenon.

2.2. Training-Free Sampling

To reduce the inference time with a trained network, there have been many advanced samplers to accelerate DDPM [8].

Song et al. [26] show that using Stochastic Differential Equation (SDE) for sampling has a marginally equivalent probability Ordinary Differential Equations (ODE). And then, DDIM [25] constructs a class of non-Markovian diffusion processes that realize skip-step sampling. PNDN [16] uses pseudo numerical to accelerate the deterministic sampling process. DEIS [39] and DPMSolver [17] improve upon DDIM by numerically approximating the score functions within each discretized time interval.

Meanwhile, several work have focused on speeding up stochastic sampling. For example, Gotta Go Fast [11] utilizes adaptive step sizes to speed up SDE sampling, and Lu et al. [18] converts the higher-order ODE solver into an SDE sampler to address the instability issue.

While these samplers have demonstrated efficacy in image generation, their impact on motion diffusion models remains unexplored. In this work, we evaluate them to find the most appropriate one for motion generation.

2.3. Footskate Cleanup

In order to generate realistic motions in computer animation, various methods have been developed to improve footskate issue.

Edge [29] embeds the foot contact term into the action representation for training and applies Contact Consistency Loss as a constraint to keep the physical plausibility of motion. RFC [34], Drop [10] and Physdiff [35] uses reinforcement learning to constrain the physical states of actions, such as ground force reaction and collision situations to get a realism motion. UnderPressure [19] and GroundLink [7] respectively collect foot force datasets during motion. UnderPressure [19] also utilizes this dataset to train a network capable of predicting vertical ground reaction forces. Based on this, UnderPressure proposes a foot skating cleanup method.

3. Preliminaries

The pipeline of Diffusion model [8] involve three interconnected processes: a **forward process** that gradually diffuses noise into sample, a **reverse process** that optimizes a network to eliminate the above perturbation, and an **inference process** that utilizes the trained network to iteratively denoise noisy sample.

Specifically, a motion denoising network is first trained to predict the original motion x_0 from the noisy motion x_t : randomly select a ground-truth motion x_0 and a diffusion timestep $t \sim U[0, T]$, T being the maximum timestep. And then the noisy motion x_t after t -step diffusion is gained by Equation 1,

$$x_t = \sqrt{\bar{\alpha}_t}x_0 + \sqrt{1 - \bar{\alpha}_t}\epsilon \quad (1)$$

where ϵ is a Gaussian noise. $\sqrt{\bar{\alpha}_t}$ and $\sqrt{1 - \bar{\alpha}_t}$ are the strengths of signal and noise, respectively. When $\sqrt{\bar{\alpha}_t}$ is small enough, we can approximate $x_t \sim \mathcal{N}(0, I)$.

Next, given a motion-denoising model $\mathbf{G}_\theta(x_t, t, c)$ for predicting the original sample, parameterized by θ , the optimization can be formulated as follows:

$$\min_{\theta} E_{t \sim U[0, T], x_0 \sim p_{data}} \|\mathbf{G}_\theta(x_t, t, c) - x_0\|_2^2 \quad (2)$$

In the inference process, a trained motion-denoising network can progressively generate samples from noise with various samplers. For instance, DDPM [8] iteratively denoise the noisy data from t to a previous timestep t' , as shown in Algorithm 1.

Algorithm 1 Inference

Given a text prompt c
 $\mathbf{x}_t \sim \mathcal{N}(0, \mathbf{I})$
for $t = T$ to 1 **do**
 $\tilde{\mathbf{x}}_0 = \mathbf{G}(\mathbf{x}_t, t, c)$
 $\epsilon \sim \mathcal{N}(0, I)$ if $t > 1$, else $\epsilon = 0$
 $\mathbf{x}_{t-1} = \frac{\sqrt{\bar{\alpha}_{t-1}}\beta_t}{1-\bar{\alpha}_t}\tilde{\mathbf{x}}_0 + \frac{\sqrt{\alpha_t(1-\bar{\alpha}_{t-1})}}{1-\bar{\alpha}_t}\mathbf{x}_t + \tilde{\beta}_t\epsilon$
end for
return \mathbf{x}_0

4. Method

Through comprehensive exploratory experiments conducted on diffusion-based motion generation, we propose a novel diffusion framework, named StableMoFusion, as illustrated in Figure 2, to facilitate robust and efficient motion generation. This section begins with our investigation on the architecture of motion-denoising networks. Next, we discuss several training strategies pivotal for enhancing model performance in Section 4.2. Subsequently, we introduce our improvements in the inference process in Section 4.3, tailored to enable efficient inference. Lastly, we discuss and present a solution to the footskate issue in Section 4.4.

4.1. Model Architecture

Most existing work use Transformer [30]-based architectures as the motion-denoising network; however, it remains questionable whether these architectures are best for diffusion-based motion generation. In this subsection, we will present three new network architectures fine-tuned for the motion generation task: Conv1D UNet [4, 13], Diffusion Transformer (DiT) [20] and the latest Retentive Network (RetNet) [27].

4.1.1 Conv1D UNet

Baseline We chose the Conv1D UNet with AdaGN [5] and skip connections in GMD [13] as the Conv1D UNet baseline and modify the structure to a canonical Unet structure, which consist of four downsampling stages. The motion length n is successively reduced from N to $\lfloor N/8 \rfloor$, and then the corresponding up-sampling phase is used to up-sample. There are two residual Conv1D blocks for each down-sampling or up-sampling stage, with a single block shown as Figure 3 (a).

Block Adjustment We introduce Residual Linear Multi-Head Cross-Attention after each block to effectively integrate textual cues, and dropout is incorporated into the original Conv1D block to enhance model generalization, as shown in Figure 3 (b). In the baseline block, text prompts

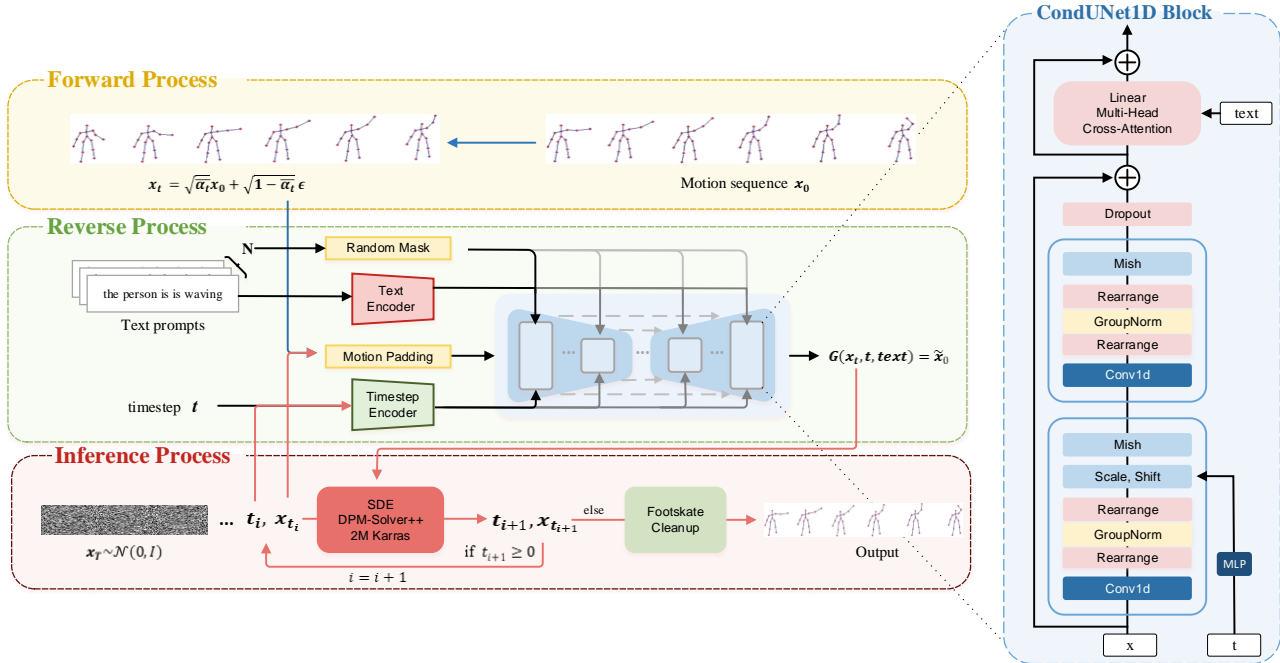


Figure 2. Overview of StableMoFusion, which is composed of a diffusion forward process, a reverse process on CondUNet1D motion-denoising network, and an efficient inference. The colors of the arrows indicate different stages: blue for training, red for inference, and black for both.

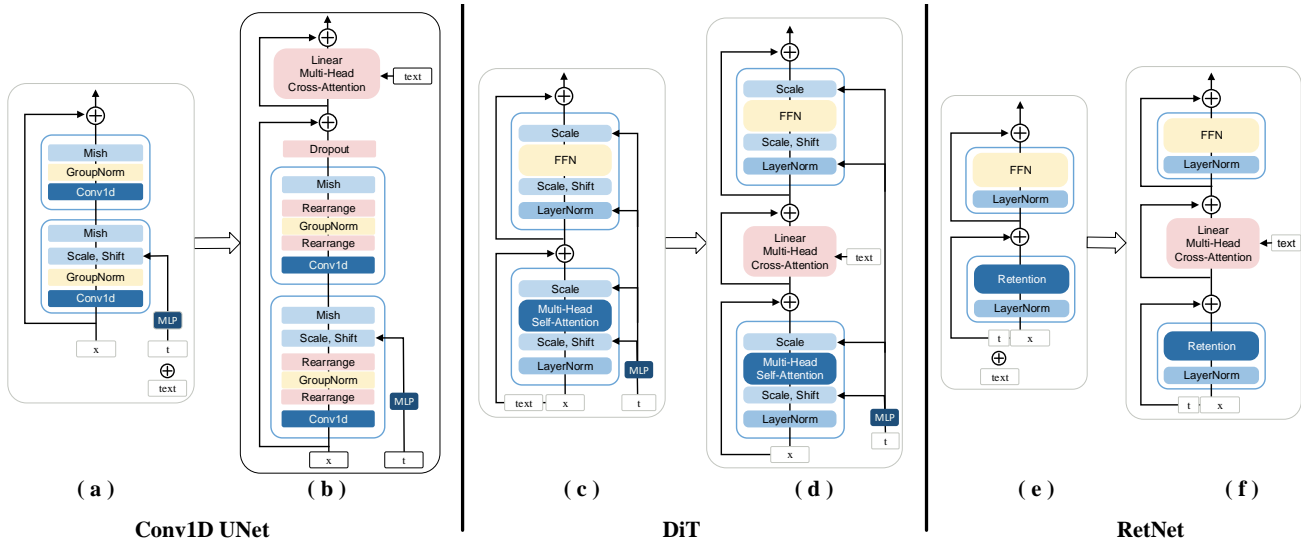


Figure 3. Visualization of the block structure and their adjustments of Conv1D UNet, DiT and RetNet. Pink blocks indicate structures that have been added or modified.

are encoded with timesteps and integrated into motion coding using a simple formula: $x \cdot (1 + scale) + shift$. However, this approach doesn't effectively incorporate textual cues into motion sequences because it applies uniform operations across the entire sequence. In diffusion pipelines, noise uniformly affects the entire sequence, resulting in consistent mappings between motion frames and timesteps.

However, since each frame's motion corresponds to distinct textual cues, a straightforward "scale and shift" approach is insufficient for injecting textual information. Our solution employs an attention mechanism to dynamically focus each motion frame on its associated textual information. Residual connections help mitigate potential computation biases introduced by cross attention.

GroupNorm Tweak We rearranged the data before and after applying Group Normalization, as depicted in Figure 3 (b), to minimize the impact of padded data during network forward propagation. When testing the adapted Conv1D UNet on datasets like KIT-ML with varying sequence lengths, we noticed a significant performance drop. This suggests that the model struggles with datasets containing extensive padding. Further investigation revealed that implementing Group Normalization within the baseline block caused this issue. Since Conv1D operates along the temporal dimension, directly applying Group Normalization to the input disrupted the differentiation between padded and non-padded data, affecting loss computation and gradient descent.

4.1.2 Diffusion Transformer

Baseline To explore the effectiveness of the DiT structure for motion generation, we replace the Vision Transformer used for images in the DiT with self-attention used for motion data as the baseline, with the basic block structure shown in Figure 3 (c). For text-to-motion generation, we embed text prompts via the CLIP [22] encoder and project them into token concatenated with motion embeddings for self-attention. It scales and shifts the motion embedding before and after each autoregressive computation using timestep, which ensures the motion denoising trajectory closely aligned with the timestep.

Block Adjustment We have also tried to incorporate Linear Multi-Head Cross-Attention into the DiT framework, as shown in Figure 3 (d). This adjustment allows for a more nuanced fusion of textual cues with motion dynamics than fusing all the text information into the one-dimensional text embedding in baseline, which enhances the coherence and relevance of generated motion sequences.

4.1.3 Retentive Network

Baseline Our RetNet baseline follows a straightforward implementation similar to MDM, where the timesteps encoding is concatenated with the textual projection to form tokens, which are then fed along with motion embeddings into RetNet, with its basic block shown in Figure 3 (e). RetNet incorporates a gated multi-scale retention mechanism, which enhances information retention and processing capabilities, thereby enabling nuanced comprehension and generation of motion sequences. Through our investigation, we aim to ascertain the feasibility of leveraging RetNet for motion generation tasks.

Block Adjustment To further integrate textual information, we also employ Linear Multi-Head Cross-Attention

between retention and FFN, as shown in Figure 3 (f). By segregating temporal and textual features, our approach aims to preserve the distinct characteristics of each modality and allow the model to independently learn and leverage relevant cues for motion generation. This separation enhances the model’s interpretability and flexibility, enabling it to better capture the intricacies of both temporal dynamics and semantic context.

4.1.4 Final Model Architecture

Ultimately, we choose the Conv1D UNet with block adjustment and GroupNorm tweak as the motion-denoising model of StableMoFusion, as shown in Figure 2. We call this network as CondUNet1D. Both DiT and RetNet use the idea of attention to activate the global receptive field in the temporal dimension, which benefits the modeling of long-range dependency. The receptive field of Conv1D UNet is mainly in the convolution kernel window, promoting a coherent and smooth transition between frames. We tend to prioritize smoother generation in current applications of motion generation.

In our StableMoFusion, we set the base channel and channel multipliers of UNet to 512 and [2,2,2,2] respectively. For text encoder, we leverage pre-trained CLIP [22] token embeddings, augmenting them with four additional transformer encoder layers, the same as MotionDiffuse [37], with a latent text dimension of 256. For timesteps encoder, it is implemented using position encoding and two linear layers, the same as StableDiffusion [23], with a latent time dimension of 512.

4.2. Training Strategies

Recent research has shown that key factors in the training strategies of the diffusion model affect the learning pattern and its generative performance [2]. In this subsection, we will analyze the impact of two empirically valid training strategies on diffusion-based motion generation: exponential moving average and classifier-free guidance.

4.2.1 Exponential Moving Average

Exponential Moving Average (EMA) calculates a weighted average of a series of model weights, giving more weight to recent data. Specifically, assume the weight of the model at time t as θ_t , then the EMA formulated as: $v_t = \beta \cdot v_{t-1} + (1 - \beta) \cdot \theta_t$, where v_t denotes the average of the network parameters for the first t iterations ($v_0 = 0$), and β is the weighted weight value.

During the training of the motion-denoising network, the network parameters change with each iteration, and the motion modeling oscillates between text-motion consistency and motion quality. Therefore, the use of EMA can smooth

out the change process of these parameters, reduce mutations and oscillations, and help to improve the stability ability of the motion-denoising model.

4.2.2 Classifier-Free Guidance

To further improve the generation quality, we use Classifier-Free Guidance (CFG) to train the motion-denoising generative model. By training the model to learn both conditioned and unconditioned distributions (e.g., setting $c = \emptyset$ for 10% of the samples), CFG ensures that the models can effectively capture the underlying data distribution across various conditions. In inference, we can trade-off text-motion consistency and fidelity using s :

$$G_s(x_t, t, c) = G(x_t, t, \emptyset) + s \cdot (G(x_t, t, c) - G(x_t, t, \emptyset)) \quad (3)$$

This ability to balance text-motion consistency and fidelity is crucial for producing varied yet realistic outputs, enhancing the overall quality of generated motion.

4.3. Efficient Inference

Time-consuming inference time remains a major challenge for diffusion-based approaches. To address this problem, we improve inference speed by integrating four efficient and training-free tricks in the inference process: 1) efficient sampler, 2) embedded-text cache, 3) parallel CFG computation, and 4) low-precision inference.

4.3.1 Efficient Sampler

We integrate the SDE variant of second-order DPM-Solver++ sampler (SDE DPM-Solver++ 2M) into diffusion-based motion generation to reduce denoising iterations. DPM-Solver is a high-order solver for diffusion stochastic differential equations (SDEs), which implies additional noise will be introduced during the iterative sampling. Thereby, stochasticity of its sampling trajectories helps to reduce the cumulative error [33], which is crucial for the realism of generated motion. In addition, we adopt the Karras Sigma [12] to set discrete timesteps. This method leverages the theory of constant-velocity thermal diffusion to determine optimal timesteps, thereby maximizing the efficiency of motion denoising within a given number of iterations.

4.3.2 Embedded-text Cache

We integrate the Embedded-text Cache mechanism into the inference process to avoid redundant calculations. In diffusion-based motion generation, the text prompt remain unchanged across iterations, resulting in same embedded text in each computation of the denoising network. Specifically, we compute the text embedding initially and subsequently utilize the embedded text directly in each network

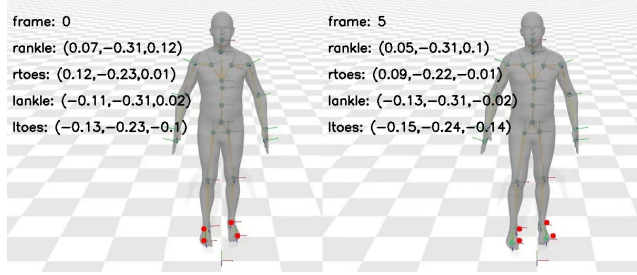


Figure 4. Red: the foot joints as 0th frame. Green: the corresponding keypoints. At 5th frame, the offset of red and green points indicate the footskate phenomenon.

forward, thereby reducing computational redundancy and speeding up inference.

4.3.3 Parallel CFG Computation

We implement the inference process of CFG in parallel to speed up the single iteration calculation while maintaining model generation performance. Due to the CFG mechanism Equation 3, in each iterative step during inference, it is necessary to execute a conditional and an unconditional denoising, respectively, using the trained motion network, and then sum up the results.

4.3.4 Low-precision Inference

We utilize half-precision floating point (FP16) computation during inference to accelerate processing. Newer hardware supports enhanced arithmetic logic units for lower-precision data types. By applying parameter quantization, we convert FP32 computations to lower-precision formats, effectively reducing computational demands, parameter size, and memory usage of the model.

4.4. Footskate Reduction

Figure 4 shows an example for the foot skating phenomenon. The motion frame rate is 20. The two frames in the figure have a time difference of 0.25s. Based on our life experience, it is difficult to complete a motion and return to the original pose within 0.25s. Although the foot postures in the two frames remain unchanged, there are changes in the positions of the joints, as observed from the variations in joint position values and their distances relative to red points. For this motion, what we expect is that the feet are anchored at the same point. Typically, choosing the foot position of middle frames during foot skating as the fixed point minimizes the impact on the adjacent frames.

The key to eliminating foot skating is to first identify the foot joints and frame ranges where foot skating occurs, and then anchor those keypoints at their positions p in the intermediate frames. We formulate this constraint as a loss

term shown in Equation 4 where j indicates joint and f is frame ranges.

$$L_{foot} = \sum_j^{J_{skating}} \sum_f^{F_{skating}} (P_j - p) \quad (4)$$

$J_{skating}$ contains all the joints where foot skating may occur, specifically including right ankle, right toes, left ankle and left toes. $F_{skating}$ is a collection of all frame ranges of the joint j . P_j means the positions of joint j . We incorporate Equation 4 to a gradient descent algorithm to correct foot skating motion.

Following UnderPressure [19], we use vertical ground reaction forces (vGRFs) to identify foot joint j and its skating frames f . The vGRFs prediction model of UnderPressure V_{23} requires motion of a predefined 23 joints skeleton S_{23} , which is different from our motion data. In our work, we utilize HumanML3D[6] with 22 skeletal joints S_{22} and KIT-ML [21] motion with 21 skeletal joints. The subsequent foot skating cleanup primarily focused on HumanML3D. We transferred the pre-trained weights of V_{23} to our own model V_{22}^θ using the constraints Equation 5, enabling us to directly predict the vertical ground reaction forces for HumanML3D motions. P is keypoints of HumanML3D motion. $P_{S_{23}}$ is the result of retargeting P to skeleton S_{23} .

$$\min_{\theta} \|V_{22}^\theta(P) - V_{23}(P_{S_{23}})\|_2^2 \quad (5)$$

$$L = \omega_q L_{pose} + \omega_f L_{foot} + \omega_t L_{trajectory} + \omega_v L_{vGRFs} \quad (6)$$

$$L_{foot} = L_{foot}(P, \hat{P}, V_{23}, P_{S_{23}}) \quad (7)$$

$$L_{vGRFs} = L_{vGRFs}(P, \hat{P}, V_{22}^\theta) \quad (8)$$

Drawing inspiration from UnderPressure [19], we use foot contact loss L_{foot} to fix contact joints, pose loss L_{pose} and trajectory loss $L_{trajectory}$ to keep the semantic integrity of motion, vGRFs loss L_{vGRFs} to keep valid foot pose. Our supplementary material provides detailed definitions of these loss terms. The final definition of our loss function is as Equation 6 [19] where $\omega_q, \omega_f, \omega_t, \omega_v$ are weights of its loss item. P is keypoints of footskating motion and \hat{P} is the result keypoints after footskate cleanup.

Through our method, the footskate cleanup process can be generalized to various skeletal motions.

In a few cases, motion corrected by Equation 6 may occurs unreasonable or unrealistic poses. The diffusion model trained on a large amount of motion data learns the prior knowledge of real motions and has the ability to correct the invalid motions.

Therefore, we use our pretrained diffusion model to correct such cases. Motivated by OmniControl [32] and Physdiff [35], we incorporates footskate cleaning method into the diffusion denoising process, denote as StableMoFusion*.

5. Experiments

5.1. Dataset and Evaluation Metrics

We use HumanML3D [6] and KIT-ML [21] dataset for our experiments. HumanML3D Dataset contains 14,646 motions and 44,970 motion annotations. KIT Motion Language Dataset contains 3,911 motions and 6,363 natural language annotations.

The evaluation metrics can be summarized into four key aspects: 1) Motion Realism: Frechet Inception Distance (FID), which evaluates the similarity between generated and ground truth motion sequences using feature vectors extracted by a pre-trained motion encoder [6]. 2) Text match: R Precision calculates the average top-k accuracy of matching generated motions with textual descriptions using a pre-trained contrastive model [6]. 3) Generation diversity: Diversity measures the average joint differences across generated sequences from all test texts. Multi-Modality quantifies the diversity within motions generated for the same text. 4) Time costs: Average Inference Time per Sentence (AITS) [3] measures the inference efficiency of diffusion models in seconds, considering generation batch size as 1, without accounting for model or data loading time.

In all of our experiments, FID and R Precision are the principal metrics we used to conduct our analysis and draw conclusions.

5.2. Implements Details

For training, we use DDPM [8] with $T = 1,000$ denoising steps and variances β_t linearly from 0.0001 to 0.02 in the forward process. And we use AdamW with an initial learning rate of 0.0002 and a 0.01 weight decay to train the sample-prediction model for 50,000 iterations at batch size 64 on an RTX A100. Meanwhile, learning rate reduced by 0.9 per 5,000 steps. On gradient descent, clip the gradient norm to 1. For CFG, setting $c = \emptyset$ for 10% of the samples.

For inference, we use the SDE variant of second-order DPM-Solver++ [18] with Karras Sigmas [12] in inference for sampling 10 steps. The scale for CFG is set to 2.5.

5.3. Quantitative Results

We compare our StableMoFusion with several state-of-the-art models, including T2M [6], MDM [28], MLD [3], MotionDiffuse [37], T2M-GPT [36], MotionGPT [9], ReMoDiffuse [38], M2DM [14] and fg-T2M [31]. on the HumanML3D [6] and KIT-ML [21] datasets in Table 2 and Table 3, respectively. Most results are borrowed from their own paper and we run the evaluation 20 times and \pm indicates the 95% confidence interval.

Our method achieves the state-of-the-art results in FID and R Precision (top k) on the HumanML3D dataset, and also achieves good results on the KIT-ML dataset: the best R Precision (top k) and the second best FID. This

Table 2. Quantitative results on the HumanML3D test set. The right arrow \rightarrow means the closer to real motion the better. **Red** and **Blue** indicate the best and the second best result.

Method	FID \downarrow	R Precision \uparrow			Diversity \rightarrow	Multi-modality \uparrow
		top1	top2	top3		
Real	0.002 \pm .000	0.511 \pm .003	0.703 \pm .003	0.797 \pm .002	9.503 \pm .065	-
T2M [6]	1.067 \pm .002	0.457 \pm .002	0.639 \pm .003	0.743 \pm .003	9.188 \pm .002	2.090 \pm .083
MDM [28]	0.544 \pm .044	0.320 \pm .005	0.498 \pm .004	0.611 \pm .007	9.599 \pm .086	2.799 \pm .072
MLD [3]	0.473 \pm .013	0.481 \pm .003	0.673 \pm .003	0.772 \pm .002	9.724 \pm .082	2.413 \pm .079
MotionDiffuse [37]	0.630 \pm .001	0.491 \pm .001	0.681 \pm .001	0.782 \pm .001	9.410 \pm .049	1.553 \pm .042
GMD [13]	0.212	-	-	0.670	9.440	-
T2M-GPT [36]	0.116 \pm .004	0.491 \pm .003	0.680 \pm .003	0.775 \pm .002	9.761 \pm .081	1.856 \pm .011
MotionGPT [9]	0.232 \pm .008	0.492 \pm .003	0.681 \pm .003	0.778 \pm .002	9.528 \pm .071	2.008 \pm .084
ReMoDiffuse [38]	0.103 \pm .004	0.510 \pm .005	0.698 \pm .006	0.795 \pm .004	9.018 \pm .075	1.795 \pm .043
M2DM [14]	0.352 \pm .005	0.497 \pm .003	0.682 \pm .002	0.763 \pm .003	9.926 \pm .073	3.587 \pm .072
Fg-T2M [31]	0.243 \pm .019	0.492 \pm .002	0.683 \pm .003	0.783 \pm .002	9.278 \pm .072	1.614 \pm .049
StableMoFusion (Ours)	0.098 \pm .003	0.553 \pm .003	0.748 \pm .002	0.841 \pm .002	9.748 \pm .092	1.774 \pm .051

Table 3. Quantitative results on the KIT-ML test set. The right arrow \rightarrow means the closer to real motion the better. **Red** and **Blue** indicate the best and the second best result.

Method	FID \downarrow	R Precision \uparrow			Diversity \rightarrow	Multi-modality \uparrow
		top1	top2	top3		
Real Motion	0.031 \pm .004	0.424 \pm .005	0.649 \pm .006	0.779 \pm .006	11.08 \pm .097	-
T2M [6]	2.770 \pm .109	0.370 \pm .005	0.569 \pm .007	0.693 \pm .007	10.91 \pm .119	1.482 \pm .065
MDM [28]	0.497 \pm .021	0.164 \pm .004	0.291 \pm .004	0.396 \pm .004	10.847 \pm .109	1.907 \pm .214
MLD [3]	0.404 \pm .027	0.390 \pm .008	0.609 \pm .008	3.204 \pm .027	10.80 \pm .117	2.192 \pm .071
MotionDiffuse [37]	1.954 \pm .062	0.417 \pm .004	0.621 \pm .004	0.739 \pm .004	11.10 \pm .143	0.730 \pm .013
T2M-GPT [36]	0.514 \pm .029	0.416 \pm .006	0.627 \pm .006	0.745 \pm .006	10.921 \pm .108	1.570 \pm .039
MotionGPT [9]	0.510 \pm .016	0.366 \pm .005	0.558 \pm .004	0.680 \pm .005	10.35 \pm .084	2.328 \pm .117
ReMoDiffuse [38]	0.155 \pm .006	0.427 \pm .014	0.641 \pm .004	0.765 \pm .055	10.80 \pm .105	1.239 \pm .028
M2DM [14]	0.515 \pm .029	0.416 \pm .004	0.628 \pm .004	0.743 \pm .004	11.417 \pm .97	3.325 \pm .37
Fg-T2M [31]	0.571 \pm .047	0.418 \pm .005	0.626 \pm .004	0.745 \pm .004	10.93 \pm .083	1.019 \pm .029
StableMoFusion (Ours)	0.258 \pm .029	0.445 \pm .006	0.660 \pm .005	0.782 \pm .004	10.936 \pm .077	1.362 \pm .062

demonstrates the ability of StableMoFusion to generate high-quality motions that align with the text prompts. On the other hand, while some methods excel in diversity and multi-modality, it’s crucial to anchor these aspects with accuracy (R-precision) and precision (FID) to strengthen their persuasiveness. Otherwise, diversity or multimodality becomes meaningless if the generated motion is bad. Therefore, our StableMoFusion achieves advanced experimental results on two datasets and shows robustness in terms of model performance.

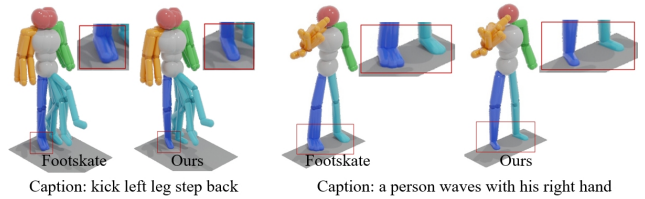


Figure 5. Visualization comparison results before and after our footskate cleanup. The red bounding box shows details of skating feet.

5.4. Qualitative Result

Figure 5 shows the visual results of our footskate cleanup method, StableMoFusion*. The red bounding box of footskate motion clearly has multiple foot outlines, whereas ours shows only one. The comparison graph shows the effectiveness of our method for cleaning footskate. Directly applying the footskate cleanup method of UnderPressure [19] to our motion would result in motion distortion, while our method effectively avoids such deformation. In our supplementary material, we will further present a comparison between our method and the UnderPressure method by videos to illustrate it.

5.5. Inference Time

We calculate AITS of StableMoFusion and ReMoDiffuse [38] with the test set of HumanML3D[6] on Tesla V100 as MLD [3] does, the other results of Figure 1 are borrowed from [3]. For instance, MDM [28] with CFG requires 24.74s for average inference; MotionDiffuse [37] without CFG uses condition encoding cache and still requires 14.74s of average inference. While the MLD [3] reduces the average inference time to 0.217s by applying DDIM50 in latent space, we find this approach lacks the ability to edit and control motion by manipulating the model input.

To tackle this, we employ 1) efficient sampler, 2) embedded-text cache, 3) parallel CFG computation, and 4) low-precision inference to reduce iteration counts and network latency. As shown in Figure 1, our StableMoFusion significantly shortens the inference time and achieves higher performance within the original motion space.

However, it remains incontrovertible that StableMoFusion’s inference speed trails behind that of MLD, and fails to meet the industry’s real-time standard with an average inference time of 0.5s. Thus, our future work will focus on acceleration: the inference time of StableMoFusion is currently tied to the computation of the network, and we will further investigate how to scale down the model and how to reduce single-step latency in inference.

5.6. Ablation

5.6.1 Network Architecture

We evaluate and compare all the architectures mentioned in Section 4.1 with the same training and inference pipeline. For a fair comparison, all methods use the real motion length from the ground truth to clip generated motion and seed(0) for one evaluation. As Table 4 show, each network enhancement in cross-attention has demonstrated performance enhancements, elucidating its pivotal role in augmenting model efficacy and effectiveness. Among them, Conv1D UNet achieves the best generation performance. And fine-tuning Conv1D UNet’s GroupNorm can effectively improve its performance on the KIT-ML dataset, re-

ducing the FID by about 64%. It also proves that the Goup-Norm tweak on UNet is mainly useful for the dataset with dispersed length distributions, such as KIT-ML dataset.

Table 4. Comparison of various architectures and adjustments.

Dataset	Network	FID ↓	R Precision (top3) ↑
HumanML3D	Conv1D UNet baseline	0.245	0.780
	+ cross-attention	0.074	0.821
	+ GroupNorm Tweak	0.089	0.840
	DiT baseline	0.884	0.711
	+ cross-attention	0.113	0.787
	RetNet baseline	1.673	0.740
	+ cross-attention	0.147	0.853
KIT-ML	Conv1D UNet+ cross-attention	0.658	0.756
	+ GroupNorm Tweak	0.237	0.780

5.6.2 Effective Inference

By using the SDE variant of second-order DPM-Solver++ with Karras sigma, the inference process of diffusion-based motion generation is able to significantly reduce the minimum number of iterations required for generation from 1000 to 10 while enhancing the quality of generated motions, approximately 99% faster than the original inference process, as shown in Table 5.

The application of embedded text caching and parallel CFG further reduces the average inference time by about 0.3s and 0.15s, respectively. Our experiments also show that reducing the computational accuracy of the motion-denoising model by half, from FP32 to FP16, does not adversely affect the generation quality. This suggests that 32-bit precision is redundant for motion generation task.

Table 5. The progressive effect of each efficient and training-free trick of StableMoFusion in inference process.

Method	FID↓	R Precision (top3)↑	AITS↓	Inference Steps↓
base (DDPM1000)	1.251	0.760	99.060	1000
+ Efficient Sampler	0.076	0.836	1.004(-99%)	10
+ Embedded-text Cache	0.076	0.836	0.690(-31%)	10
+ Parallel CFG	0.076	0.836	0.544(-21%)	10
+ FP16	0.076	0.837	0.499(-8%)	10

6. Conclusion

In this paper, we propose a robust and efficient diffusion-based motion generation framework, StableMoFusion, which uses Conv1DUNet as a motion-denoising network and employs two effective training strategies to enhance the network’s effectiveness, as well as four training-free tricks to achieve efficient inference. Extensive experimental results show that our StableMoFusion performs favorably against current state-of-the-art methods. Furthermore, we

propose effective solutions for time-consuming inference and footskate problems, facilitating diffusion-based motion generation methods for practical applications in industry.

References

- [1] Samaneh Azadi, Akbar Shah, Thomas Hayes, Devi Parikh, and Sonal Gupta. Make-an-animation: Large-scale text-conditional 3d human motion generation. *arXiv preprint arXiv:2305.09662*, 2023. [1](#)
- [2] Hanqun Cao, Cheng Tan, Zhangyang Gao, Yilun Xu, Guangyong Chen, Pheng-Ann Heng, and Stan Z Li. A survey on generative diffusion model. *arXiv preprint arXiv:2209.02646*, 2022. [5](#)
- [3] Xin Chen, Biao Jiang, Wen Liu, Zilong Huang, Bin Fu, Tao Chen, and Gang Yu. Executing your commands via motion diffusion in latent space. In *Proceedings of the IEEE/CVF Conference on Computer Vision and Pattern Recognition*, pages 18000–18010, 2023. [1](#), [2](#), [7](#), [8](#), [9](#)
- [4] Rishabh Dabral, Muhammad Hamza Mughal, Vladislav Golyanik, and Christian Theobalt. Mofusion: A framework for denoising-diffusion-based motion synthesis. In *Proceedings of the IEEE/CVF Conference on Computer Vision and Pattern Recognition*, pages 9760–9770, 2023. [1](#), [2](#), [3](#)
- [5] Prafulla Dhariwal and Alexander Nichol. Diffusion models beat gans on image synthesis. *Advances in neural information processing systems*, 34:8780–8794, 2021. [3](#)
- [6] Chuan Guo, Shihao Zou, Xinxin Zuo, Sen Wang, Wei Ji, Xingyu Li, and Li Cheng. Generating diverse and natural 3d human motions from text. In *Proceedings of the IEEE/CVF Conference on Computer Vision and Pattern Recognition*, pages 5152–5161, 2022. [7](#), [8](#), [9](#), [12](#)
- [7] Xingjian Han, Benjamin Senderling, Stanley To, Deepak Kumar, Emily Whiting, and Jun Saito. Groundlink: A dataset unifying human body movement and ground reaction dynamics. In *ACM SIGGRAPH Asia 2023 Conference Proceedings*, pages 1–10, 2023. [3](#)
- [8] Jonathan Ho, Ajay Jain, and Pieter Abbeel. Denoising diffusion probabilistic models. *Advances in neural information processing systems*, 33:6840–6851, 2020. [2](#), [3](#), [7](#), [13](#)
- [9] Biao Jiang, Xin Chen, Wen Liu, Jingyi Yu, Gang Yu, and Tao Chen. Motiongpt: Human motion as a foreign language. *Advances in Neural Information Processing Systems*, 36, 2024. [7](#), [8](#)
- [10] Yifeng Jiang, Jungdam Won, Yuting Ye, and C Karen Liu. Drop: Dynamics responses from human motion prior and projective dynamics. *SIGGRAPH Asia*, 2023. [3](#)
- [11] Alexia Jolicœur-Martineau, Ke Li, Rémi Piché-Taillefer, Tal Kachman, and Ioannis Mitliagkas. Gotta go fast when generating data with score-based models. *arXiv preprint arXiv:2105.14080*, 2021. [2](#)
- [12] Tero Karras, Miika Aittala, Timo Aila, and Samuli Laine. Elucidating the design space of diffusion-based generative models. *Advances in Neural Information Processing Systems*, 35:26565–26577, 2022. [6](#), [7](#), [13](#), [14](#)
- [13] Korrawe Karunratanakul, Konpat Preechakul, Supasorn Suwajanakorn, and Siyu Tang. Gmd: Controllable human motion synthesis via guided diffusion models. *arXiv preprint arXiv:2305.12577*, 2023. [2](#), [3](#), [8](#)
- [14] Hanyang Kong, Kehong Gong, Dongze Lian, Michael Bi Mi, and Xinchao Wang. Priority-centric human motion generation in discrete latent space. In *Proceedings of the IEEE/CVF International Conference on Computer Vision*, pages 14806–14816, 2023. [7](#), [8](#)
- [15] Jiefeng Li, Siyuan Bian, Chao Xu, Zhicun Chen, Lixin Yang, and Cewu Lu. Hybrik-x: Hybrid analytical-neural inverse kinematics for whole-body mesh recovery. *arXiv preprint arXiv:2304.05690*, 2023. [12](#)
- [16] Luping Liu, Yi Ren, Zhijie Lin, and Zhou Zhao. Pseudo numerical methods for diffusion models on manifolds. In *International Conference on Learning Representations*, 2021. [2](#), [13](#)
- [17] Cheng Lu, Yuhao Zhou, Fan Bao, Jianfei Chen, Chongxuan Li, and Jun Zhu. Dpm-solver: A fast ode solver for diffusion probabilistic model sampling in around 10 steps. *Advances in Neural Information Processing Systems*, 35:5775–5787, 2022. [2](#), [13](#)
- [18] Cheng Lu, Yuhao Zhou, Fan Bao, Jianfei Chen, Chongxuan Li, and Jun Zhu. Dpm-solver++: Fast solver for guided sampling of diffusion probabilistic models. *arXiv preprint arXiv:2211.01095*, 2022. [2](#), [7](#), [13](#)
- [19] Lucas Mourot, Ludovic Hoyet, François Le Clerc, and Pierre Hellier. Underpressure: Deep learning for foot contact detection, ground reaction force estimation and footskate cleanup. *Computer Graphics Forum*, 41(8):195–206, 2022. [3](#), [7](#), [9](#)
- [20] William Peebles and Saining Xie. Scalable diffusion models with transformers. In *Proceedings of the IEEE/CVF International Conference on Computer Vision*, pages 4195–4205, 2023. [3](#)
- [21] Matthias Plappert, Christian Mandery, and Tamim Asfour. The kit motion-language dataset. *arXiv preprint arXiv:1607.03827*, 2016. [7](#)
- [22] Alec Radford, Jong Wook Kim, Chris Hallacy, Aditya Ramesh, Gabriel Goh, Sandhini Agarwal, Girish Sastry, Amanda Askell, Pamela Mishkin, Jack Clark, et al. Learning transferable visual models from natural language supervision. In *International conference on machine learning*, pages 8748–8763. PMLR, 2021. [5](#)
- [23] Robin Rombach, Andreas Blattmann, Dominik Lorenz, Patrick Esser, and Björn Ommer. High-resolution image synthesis with latent diffusion models. In *Proceedings of the IEEE/CVF conference on computer vision and pattern recognition*, pages 10684–10695, 2022. [5](#)
- [24] Yonatan Shafir, Guy Tevet, Roy Kapon, and Amit H Bermano. Human motion diffusion as a generative prior. *arXiv preprint arXiv:2303.01418*, 2023. [2](#)
- [25] Jiaming Song, Chenlin Meng, and Stefano Ermon. Denoising diffusion implicit models. In *International Conference on Learning Representations*, 2020. [2](#), [13](#)
- [26] Yang Song, Jascha Sohl-Dickstein, Diederik P Kingma, Abhishek Kumar, Stefano Ermon, and Ben Poole. Score-based generative modeling through stochastic differential equations. *arXiv preprint arXiv:2011.13456*, 2020. [2](#), [13](#)
- [27] Yutao Sun, Li Dong, Shaohan Huang, Shuming Ma, Yuqing Xia, Jilong Xue, Jianyong Wang, and Furu Wei. Retentive

- network: A successor to transformer for large language models. *arXiv preprint arXiv:2307.08621*, 2023. 3
- [28] Guy Tevet, Sigal Raab, Brian Gordon, Yonatan Shafir, Daniel Cohen-Or, and Amit H Bermano. Human motion diffusion model. *arXiv preprint arXiv:2209.14916*, 2022. 1, 2, 7, 8, 9, 12
- [29] Jonathan Tseng, Rodrigo Castellon, and C Karen Liu. Edge: Editable dance generation from music. *arXiv preprint arXiv:2211.10658*, 2022. 3
- [30] Ashish Vaswani, Noam Shazeer, Niki Parmar, Jakob Uszkoreit, Llion Jones, Aidan N Gomez, Łukasz Kaiser, and Illia Polosukhin. Attention is all you need. *Advances in neural information processing systems*, 30, 2017. 3
- [31] Yin Wang, Zhiying Leng, Frederick WB Li, Shun-Cheng Wu, and Xiaohui Liang. Fg-t2m: Fine-grained text-driven human motion generation via diffusion model. In *Proceedings of the IEEE/CVF International Conference on Computer Vision*, pages 22035–22044, 2023. 7, 8
- [32] Yiming Xie, Varun Jampani, Lei Zhong, Deqing Sun, and Huaizu Jiang. Omnicontrol: Control any joint at any time for human motion generation. In *The Twelfth International Conference on Learning Representations*, 2024. 7
- [33] Yilun Xu, Mingyang Deng, Xiang Cheng, Yonglong Tian, Ziming Liu, and Tommi Jaakkola. Restart sampling for improving generative processes. *arXiv preprint arXiv:2306.14878*, 2023. 6
- [34] Ye Yuan and Kris Kitani. Residual force control for agile human behavior imitation and extended motion synthesis. In *Advances in Neural Information Processing Systems*, 2020. 3
- [35] Ye Yuan, Jiaming Song, Umar Iqbal, Arash Vahdat, and Jan Kautz. Physdiff: Physics-guided human motion diffusion model. In *Proceedings of the IEEE/CVF International Conference on Computer Vision*, pages 16010–16021, 2023. 2, 3, 7
- [36] Jianrong Zhang, Yangsong Zhang, Xiaodong Cun, Shaoli Huang, Yong Zhang, Hongwei Zhao, Hongtao Lu, and Xi Shen. T2m-gpt: Generating human motion from textual descriptions with discrete representations. *arXiv preprint arXiv:2301.06052*, 2023. 7, 8
- [37] Mingyuan Zhang, Zhongang Cai, Liang Pan, Fangzhou Hong, Xinying Guo, Lei Yang, and Ziwei Liu. Motiondiffuse: Text-driven human motion generation with diffusion model. *arXiv preprint arXiv:2208.15001*, 2022. 1, 2, 5, 7, 8, 9, 12, 13
- [38] Mingyuan Zhang, Xinying Guo, Liang Pan, Zhongang Cai, Fangzhou Hong, Huirong Li, Lei Yang, and Ziwei Liu. Remodiffuse: Retrieval-augmented motion diffusion model. In *Proceedings of the IEEE/CVF International Conference on Computer Vision*, pages 364–373, 2023. 1, 2, 7, 8, 9
- [39] Qinsheng Zhang and Yongxin Chen. Fast sampling of diffusion models with exponential integrator. In *NeurIPS 2022 Workshop on Score-Based Methods*, 2022. 2, 13

Appendix

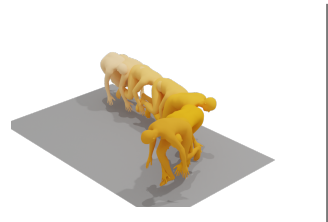

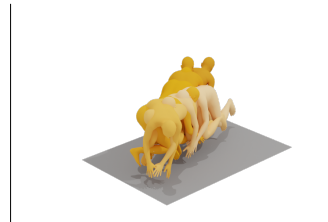

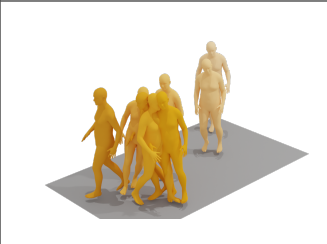

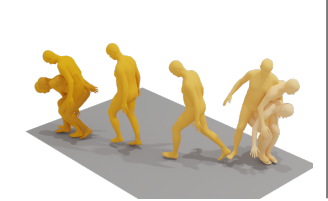
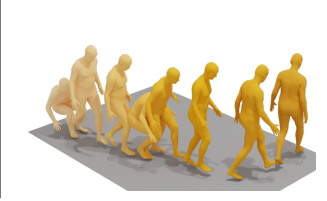
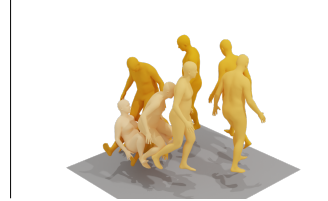
This appendix provides more qualitative results (Appendix A), detailed definitions of footskate cleanup loss (Appendix B), and additional experiments on the diffusion samplers (Appendix C).

A. Qualitative Results

Video. We have provided supplemental videos in [Project Page](#). In these supplemental videos, we show 1) comparisons of text-based motion generation with the state-of-the-art, 2) comparisons of footskate cleanup, and 3) more samples of text-conditional motion synthesis. We suggest the reader watch this video for dynamic motion results.

Sequence Figures. To facilitate visualization and explication within the text, we adopt a method akin to the previous approach, wherein the entire motion sequence is rendered into a composite image by stacking all frames, as depicted in [Table 6](#) and [Figure 6](#).

Table 6. Comparisons with the state-of-the-art methods on text-conditional motion synthesis task. All provided methods are trained on the HumanML3D [6] dataset and all samples are generated with the same text prompts and motion length.

Text Prompts	MDM [28]	MotionDiffuse [37]	StabelMoFusion (ours)
A person crawls on the ground from east to west then goes back			
A person runs back and forth			
A person stands up from laying, walks in a circle, and lays down again			

[Table 6](#) shows comparisons between our method, MDM [28], and MotionDiffuse [37]. We highlight that StableMoFusion achieves a balance between text-motion consistency and motion quality. For example, when prompted with *A person stands up from laying, walks in a clockwise circle, and lays down again*, our resultant motion encapsulates a full circular movement and concludes with the reclining action. For the prompt *A person runs back and forth*, our generated motion portrays a complete back-and-forth journey.

[Figure 6](#) provides more samplers generated from various text prompts by our StableMoFusion framework. Our framework is able to generate high-quality motions that reflect the detailed description.

B. Footskate Cleanup loss

Here we provide detailed definitions of footskate cleanup loss. The complete loss function is as [Equation 9](#). Pose loss L_{pose} minimize the mean squared error(MSE) of motion pose to keep semantic invariant. We use Euler angles to represent motion and convert keypoints to Euler angles by HybriK algorithm [15]. Trajectory loss $L_{trajectory}$ has the same function as L_{pose} by constraining velocity of root bone. Foot contact loss L_{foot} use MSE to fix foot. \hat{P} is keypoints of footskate cleaned motion. In the early stage of the algorithm, we use V_{23} to calculate target anchored points, denoted as p . VGRF loss L_{vGRFs} keeps valid foot pose by minimizing the mean squared logarithmic error.

$$L = \omega_q L_{\text{pose}} + \omega_f L_{\text{foot}} + \omega_t L_{\text{trajectory}} + \omega_v L_{\text{vGRFs}} \quad (9)$$

$$L_{\text{pose}}(P, \hat{P}) = \|\text{HybrIK}(P) - \text{HybrIK}(\hat{P})\|_2^2 \quad (10)$$

$$L_{\text{foot}}(P, \hat{P}, V_{23}, P_{S_{23}}) = \sum_{j_{23}}^{J_{\text{skating}}} \sum_{f_{23}}^{F_{\text{skating}}} (\hat{P}_j - p) \quad (11)$$

$$L_{\text{trajectory}}(P, \hat{P}) = \|(P_0^{1:H} - P_0^{0:H-1}) - (\hat{P}_0^{1:H} - \hat{p}_0^{0:H-1})\|_2^2 \quad (12)$$

$$L_{\text{vGRFs}}(P, \hat{P}, V_{22}^\theta) = \|\log(1 + V_{22}^\theta(P)) - \log(1 + V_{22}^\theta(\hat{P}))\|_2^2 \quad (13)$$

C. Additional Experiments on Samplers

In this section, we will show the effect of incorporating five experienced discrete-time samplers into the motion diffusion framework. To select the most suitable sampler for efficient inference, we initially used the pre-trained models in MotionDiffuse [37] to evaluate and analyze these samplers, namely DDPM [8], DDIM [25], DPMSolver [17, 18], PNDM [16], and DEIS [39], which preceded our development of the model architecture.

These samplers can be categorized into two groups based on whether adding additional noise in each reverse step: Ordinary Differential Equations (ODE) [12] and Stochastic Differential Equation (SDE) [26] samplers.

C.1. Experimental setup.

We use the trained models of MotionDiffus [37] to evaluate the inference effects of the five samplers on both For a fair comparison, All inference experiments use the same *batchsize* = 1024 and set *seed* = 0. Use DDPM [8] with $T = 1,000$ as control group (Ctrl).

Table 7. Comparison of samplers on MotionDiffuse using the HumanML3D test set. The minimum sampling step is selected if its FID and R Precision (top3) are within 5% of the optimal result.

	Sampler	Minimum Sampling Steps	FID ↓	R Precision (top3) ↑
ODE	DDIM	500	1.253	0.764
	PNDM	200	1.297	0.763
	DEIS	20	1.281	0.761
	DPMSolver++	20	1.235	0.764
SDE	DDPM (Ctrl)	1000	0.709	0.778
	DDPM	500	0.731	0.787
	SDE DPMSolver++	20	0.680	0.774
	SDE DPMSolver++ Karras	10	0.521	0.781

C.2. ODE Samplers

ODE samplers accelerate DDPM by solving ODEs on manifold without additional noise. These approaches construct a deterministic sampling trajectory that traverses from noise space to the target data distribution. ODE samplers have been shown to produce less discretization error than the SDE samplers, however, they will eventually reach the upper limit of their performance due to their deterministic sampling trajectories from noise to the data distribution, which leads to a certain cumulative error as shown in Table 7 and Table 8.

Although ODE samplers can significantly decrease the number of sampling steps from 1000 by a certain amount, they are only capable of generating motions with FID around 2.0 on KIT-ML dataset and FID around 1.25 on HumanML3D dataset.

C.3. SDE Samplers

Since SDE samplers introduce additional noise during the iterative inference process, the stochasticity of their sampling trajectories helps to reduce the cumulative error, which is crucial for diversity and realism in diffusion-based motion generation, as shown in Table 7 and Table 8.

SDE samplers are capable of generating higher quality motions than the ODE sampler.

Table 8. Comparison of samplers on MotionDiffuse using the KIT-ML test set. The minimum sampling step is selected if its FID and R Precision (top3) are within 5% of the optimal result.

	Sampler	Minimum Sampling Steps	FID ↓	R Precision (top3) ↑
ODE	DDIM	200	2.012	0.711
	PNDM	50	2.069	0.736
	DEIS	2	2.006	0.720
	DPMSolver++	4	1.962	0.734
SDE	DDPM (Ctrl)	1000	1.673	0.740
	DDPM	500	1.712	0.743
	SDE DPMSolver++	5	1.590	0.743
	SDE DPMSolver++ Karras	5	0.886	0.727

C.4. Karras Sigma

The Karras Sigma [12] $\sigma(t) = \sqrt{t}$ corresponds to constant-velocity thermal diffusion, which enables fast and good sampling in image synthesis. Karras sigma also improves the quality of motion diffusion generation, as shown in Table 7 and Table 8. By using Karras Sigma, the quality of the DPM-Solver++ sampler for motion generation is improved from 1.6 FID to 0.886 on KIT-ML dataset and .

Using Karras Sigma in sampler can improves the quality of motion diffusion generation.

C.5. Ablation on StableMoFusion

We also re-validated the efficiency of the selected one, SDE variant of second-order DPM-Solver++ with Karras Sigmas (SDE DPM-Solver++ Karras), compared to other samplers in our final framework, the results of which are shown in Table 9.

Note that, the minimum sampling steps vary when utilizing the same sampler across different datasets or different frameworks.

Table 9. Comparison of samplers on StableMoFusion using the KIT test set. The minimum sampling step is selected if its FID and R Precision (top3) are within 5% of the optimal result.

Sampler	Minimum Sampling Steps	FID ↓	R Precision (top3) ↑
DDIM	200	0.243	0.794
DDPM	500	0.253	0.793
SDE DPMSolver++	5	0.246	0.796
SDE DPMSolver++ Karras	10	0.209	0.780



(a) He walks forward and then turns around fast and walks back



(b) The person is striking a tennis ball unenthusiastically



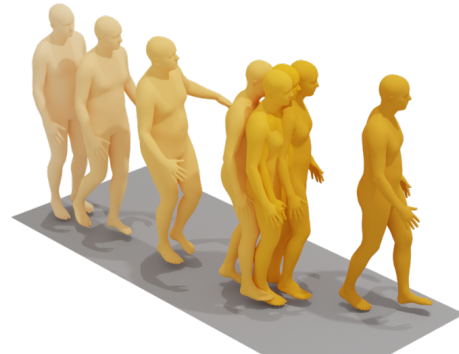
(c) The person is dancing the waltz



(d) A person walks up stairs



(e) A person is on his knees and then gets up by pushing himself up with his right hand



(f) A person walks in a left diagonal then stops with hands slightly raised



(g) A person is doing jumping jacks



(h) A person jump ropes

Figure 6. More samples of our StableMoFusion for text-to-motion synthesis.